A Closed-loop System for Artifact Mitigation in Ambulatory Electrocardiogram Monitoring

Mohammed Shoaib†
Department of Electrical Engineering
Princeton University NJ 08544
Email: mshoaib@princeton.edu

Gene Marsh, Harinath Garudadri, and Somdeb Majumdar
Qualcomm Inc.
5775 Morehouse Dr., San Diego CA 92122
Email: {gmarsh,hgarudad,smajumda}@qualcomm.com

***Abstract*—Motion artifacts interfere with electrocardiogram (ECG) detection and information processing. In this paper, we present an independent component analysis based technique to mitigate these signal artifacts. We propose a new statistical measure to enable an automatic identification and removal of independent components, which correspond to the sources of noise. For the first time, we also present a signal-dependent closed-loop system for the quality assessment of the denoised ECG. In one experiment, noisy data is obtained by the addition of calibrated amounts of noise from the MIT-BIH NST database to the AHA ECG database. Arrhythmia classification based on a state-of-the-art algorithm with the direct use of noisy data thus obtained shows sensitivity and positive predictivity values of 87.7% and 90.0%, respectively, at an input signal SNR of -9 dB. Detection with the use of ECG data denoised by the proposed approach exhibits significant improvement in the performance of the classifier with the corresponding results being 96.5% and 99.1%, respectively. In a related lab trial, we demonstrate a reduction in RMS error of instantaneous heart rate estimates from 47.2% to 7.0% with the use of 56 minutes of denoised ECG from four physically active subjects. To validate our experiments, we develop a closed-loop, ambulatory ECG monitoring platform, which consumes 2.17 mW of power and delivers a data rate of 33 kbps over a dedicated UWB link.**

I. Introduction

Recent advances in mobile computing and energy-efficient communication have enabled algorithms capable of efficient and accurate processing of data [1]. Devices which monitor dynamic physical systems, however, present large volumes of data corrupt with a wide range of signal artifacts for analysis by these algorithms; in ambulatory electrocardiogram monitoring, for instance, artifacts can result from the movement of electrodes on the surface of the skin, power line interference, muscle noise, and baseline-wander [2]. Direct processing of noisy data thus hampers the performance of algorithms, which rely on ambulatory ECG, such as those used for beat detection [3] and arrhythmia classification [2]. Efficient techniques for the selective removal of artifact sources while retaining useful signal components are thus essential to ensure accurate performance of ECG processing algorithms.

In the literature, analog and digital filtering techniques have demonstrated great success in the mitigation of noise in the ECG data, which originates from several sources [2], [4]. Motion artifacts and muscle noise, however, present a unique challenge to such signal-processing methods. Linear and non-linear filters fail to effectively remove interference from these sources since they represent noise, which is within the same time and frequency range as the ECG. Traditional filtering techniques applied to the noisy recordings may thus eliminate useful signal components and corrupt the spectral content, and thus, the morphology of the ECG.

†This work was done while the author was at Qualcomm Inc., 5775 Morehouse Dr., San Diego CA 92122

II. Background

Independent component analysis (ICA) is a method of blind source separation, which relies on the property of linear superposition of statistically independent signals. Its applicability to biomedical data has recently gained interest [5]. However, current ICA based ECG artifact mitigation algorithms rely on a visual inspection of independent components to identify those that correspond to the sources of noise [5]–[7]. Although some recent methods try to automate the identification process [8], [9], they are limited in their ability to function across the range of ECG morphologies routinely seen in clinical practice, as evidenced in standard patient databases. In this paper, we propose a robust statistical metric to enable an automatic separation of independent components, which belong to a noise space. Further, we also present a signal-dependent metric for an automatic quality assessment of the denoised ECG. To the best of our knowledge, this is the first attempt in the literature to enable such a closed-loop feedback. We demonstrate the efficacy of the proposed technique by the use of noisy ECG from extensive databases as well as from active subjects in the lab.

A. Independent Component Analysis

In this section, we provide an overview of the ICA algorithm and its applicability to denoise multi-lead ECG signals. Fig. 1 illustrates the algorithm. Given a set of k independent time domain sources $\mathbf{s} = \{s_1(t), \ldots, s_k(t)\}$, linearly mixed to produce m noisy measurements $\mathbf{x_n} = \{x_{n,1}(t), \ldots, x_{n,m}(t)\}$, according to the relationship

$$\mathbf{x_n} = \mathbf{As}, \tag{1}$$

where $\mathbf{A}$ is called the mixing matrix, the ICA algorithm provides an estimate of the de-mixing matrix $\mathbf{A_d}$ [5], [10].

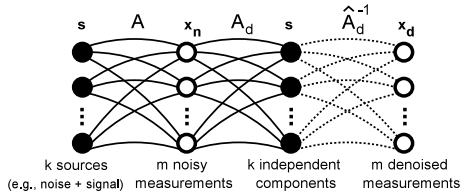

Fig. 1: Illustration of the ICA algorithm

978-3-9810801-8-6/DATE12/© 2012 EDAA

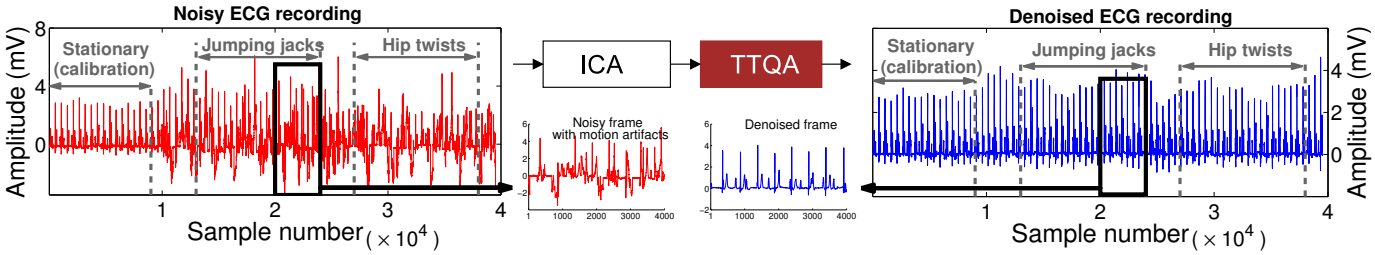

Fig. 2: TTQA facilitates an automatic elimination of noise components and a closed-loop assessment of artifact mitigation using ICA.

The set of source signals [also called independent components (ICs)] can thus be recovered as $\mathbf{s} = \mathbf{A_d x_n}$. Further, in general, $\mathbf{A}$ and $\mathbf{A_d}$ are non-stationary, non-square matrices and ideally $\mathbf{A A_d} = \mathbf{I}$.

Denoising electrocardiogram signals. In an ECG measurement system, surface potentials on the body due to electrical activity in the heart, along with the statistically independent motion artifacts, and muscle noise correspond to the source signal set $\mathbf{s}$. A linear mixture of the sources is observed as the surface ECG signal. The ICA algorithm thus makes use of noisy measurements $\mathbf{x_n}$ to estimate the independent signal sources $\mathbf{s}$ and the de-mixing matrix $\mathbf{A_d}$. In the denoising process, a modified mixing matrix $\hat{\mathbf{A}}_\mathbf{d}^{-1}$ is obtained by zeroing out columns of $\mathbf{A_d}^{-1}$ corresponding to noise sources in the estimated set of ICs. Thus, the denoised ECG measurements can be recovered as follows:

$$\mathbf{x_d} = \hat{\mathbf{A}}_\mathbf{d}^{-1}\mathbf{s}. \tag{2}$$

B. Challenges in ICA-based Denoising of ECG Data

As is evident from the above process, there are two major practical difficulties in denoising ECG signals using ICA.

1) First, it is non-trivial to automatically identify ICs in $\mathbf{s}$, which belong to a noise space.
2) Second, after zeroing out columns of $\mathbf{A}_\mathbf{d}^{-1}$, which correspond to the noise components in $\mathbf{s}$, there is no practical metric to evaluate the quality of the denoised ECG.

The first challenge above stems from the varied range of artifacts that can appear in the ECG; for example, electrode motion noise appears as irregular disturbances, whereas, muscle noise can manifest itself as a wide-band Gaussian interference. The second difficulty arises since the electrical activity of the heart at the epicardium is not directly measurable. Thus, without access to the expected denoised signal, traditional metrics such as signal-to-noise ratio (SNR) or signal-to-interference ratio (SINR) cannot be used. In this paper, we propose techniques to overcome the above challenges facilitating the process of practical ICA-based denoising.

The rest of the paper is organized as follows. In Sec. III, we describe the sub-systems used in the proposed temporally-tuned quality assessment (TTQA) algorithm. In Sec. IV, we present a validation of the TTQA algorithm based on the Physikalish-Technishe Bundesanstalt (PTB) diagnostic ECG database [11]. We then present two case studies for the application of TTQA, *viz.*, arrhythmia detection in Sec. V, followed by instantaneous heart rate (IHR) estimation in Sec. VI. Finally, we conclude in Sec. VII.

III. Temporally-tuned Quality Assessment

In this section, we introduce sub-systems, which comprise the TTQA algorithm. Fig. 2 summarizes the functionality of TTQA in the process of ICA-based ECG denoising. On the left, the figure shows a recording from channel MLII of a subject performing 60 seconds each of jumping jacks and hip twists after remaining stationary for 60 seconds. As is illustrated in the figure, ICA is used to separate statistically independent components in the ECG. After the separation process, TTQA is used for an automatic identification of the noise components, which are eliminated while simultaneously evaluating its effect on the quality of the denoised ECG in an iterative feedback loop. The resulting denoised recording thus obtained is shown at the right.

A. Automatic Identification of Noise Components

A block diagram of the proposed TTQA algorithm implemented in MATLAB is shown in Fig. 3. It comprises a Kurtosis-VarMean based module for an automatic identification of components that belong to a noise space followed by a module for closed-loop temporal clustering.

Isolation of ICs. Prior to denoising by TTQA, principal component analysis (PCA) is used for dimensionality reduction by orthogonal projection of the noisy data [10]. ICA is then applied to separate the constituent ICs. If f_s is the sampling frequency of the noisy ECG, m frames of Nf_s samples each, represented by $\mathbf{x}_n$, are processed at a time by the PCA block (N samples from one frame are illustrated in Fig. 3). ICA is then applied to separate k ICs in the noisy ECG, which are represented by $\mathbf{s}$ in the block diagram. To implement the ICA algorithm, the fastICA package [12] along with ICASSO [13] is used.

IC denoising. The k ICs thus obtained are processed by the

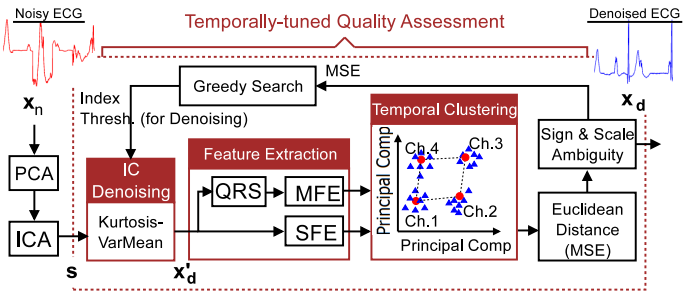

Fig. 3: The TTQA algorithm comprises an automatic separation of noise components based on kurtosis-VarMean followed by spectral or morphological feature extraction for temporal clustering.

	Kurtosis	VarMean		VarMed		VarVar	
	VALUE	VALUE	INDEX	VALUE	INDEX	VALUE	INDEX
IC#1 (noise)	0.0505	0.8248	**0.0018**	0.9323	**0.0002**	0.1734	**0.0849**
IC#2 (ECG)	0.0344	0.1111	0.0093	0.0592	**0.0017**	0.2132	**0.0470**
IC#3 (ECG)	0.3982	0.0419	0.2856	0.0043	0.4317	0.2713	0.4277
IC#4 (ECG)	0.5169	0.0221	0.7032	0.0043	0.5653	0.3421	0.4403
SINR of frame		**13.54 dB**		**11.05 dB**		**11.05 dB**	

TABLE I: IC #2 is erroneously removed by the use of a Kurtosis-VarVar based metric.

IC denoising block, which relies on thresholding a Kurtosis-VarMean index to enable an automatic identification of components, which belong to a noise space.

Kurtosis [$\mathbf{K}(\mathbf{s})$] is a fourth-order cumulant and is zero for Gaussian densities. It is defined as

$$\mathbf{K}(\mathbf{s}) = \mathbf{E}(\mathbf{s}^4) - 3\left[\mathbf{E}(\mathbf{s}^2)\right]^2 \tag{3}$$

where $\mathbf{E}(\cdot)$ is the expectation. Muscle noise, with a near Gaussian distribution, has a $\mathbf{K}(\mathbf{s})$ value much smaller than the ECG signal, and is thus clearly distinguishable. Although $\mathbf{K}(\mathbf{s})$ is a useful metric to identify continuous noise, a secondary measure is required to distinguish ICs, which originate from additional sources of noise. The VarVar metric introduced in [8] is ineffective for the identification of components, which arise due to the electrode motion noise, such as those shown in Fig. 2 and Table I. Electrode motion noise, represented by IC#1, is the only noise component present in the exemplary measurement shown in Table I.

The use of a Kurtosis-VarVar index (given by the ratio of $\mathbf{K}(\mathbf{s})$ and VarVar), described in [8], leads to a faulty elimination of IC#2 by greedy thresholding. We thus propose a new secondary metric based on the variance of IC-segment means (or VarMean, $\sigma^2_{\bar{\mathbf{Y}}}$), which exploits the quasi-periodic nature of the ECG signal components. For every component $\mathbf{s}_i$ of Nf_s samples obtained using m ECG leads, $\sigma^2_{\bar{\mathbf{Y}}}$ corresponds to the variance in the mean amplitude of N linearly spaced one-second segments. In other words, suppose $\mathbf{s}'_{it}$ and $\bar{\mathbf{s}}'_{it}$ represent a segment of f_s samples derived from $\mathbf{s}_i$ prior to time $t \in 1, 2, \ldots, T$, and its mean amplitude, respectively. $\sigma^2_{\bar{\mathbf{Y}}}$ corresponds to the variance of the set $\mathbf{y}_i = \{\bar{\mathbf{s}}'_{i1}, \bar{\mathbf{s}}'_{i1}, \ldots, \bar{\mathbf{s}}'_{iT}\}$.

ICs which arise due to the ECG signal have a smaller $\sigma^2_{\bar{\mathbf{Y}}}$ value as compared to those that originate from electrode motion artifacts. This behavior is observed since the mean amplitudes in adjacent segments of the quasi-periodic signal components are in close proximity to one another. Their $\sigma^2_{\bar{\mathbf{Y}}}$ value is thus near zero, which enables a clear distinction from the ICs in the noise space. Consequently, clean ECG frames are obtained by the use of a modified de-mixing matrix $\hat{\mathbf{A}}_\mathbf{d}$ derived by zeroing out columns of $\mathbf{A}_\mathbf{d}$, which correspond to the noise components (identified by the value of their $\mathbf{K}(\mathbf{s})/\sigma^2_{\bar{\mathbf{Y}}}$ index being below a certain threshold). The $\mathbf{K}(\mathbf{s})/\sigma^2_{\bar{\mathbf{Y}}}$ indices for the denoised ECG frames are shown in Table I; a comparison with the VarVar and VarMedian based indices is also shown. The latter two metrics, in the earlier formulation, correspond to $\bar{\mathbf{s}}'_{it}$ being equal to the variance and median of $\mathbf{s}_{it}$, respectively, instead of the mean.

Feature extraction. After every iteration of the threshold-based IC selection approach, m denoised frames, represented by $\mathbf{x}_\mathbf{d}$, are processed further for dimensionality reduction. Either of the following two methods are used to obtain m feature vectors corresponding to each of the m denoised ECG leads: (1) morphological feature extraction (MFE), where the average morphology of the denoised ECG signal, represented by $f_s/3$ samples around each beat isolated by a QRS detector, forms a feature vector, or (2) spectral feature extraction (SFE), where a feature vector is represented by the energy content in several linearly spaced bins in the frequency range $0 - f_s/2$.

Temporal clustering. Following the feature extraction process, a temporal clustering technique is used to assess the quality of the denoised ECG in each iteration.

Feature vectors derived in the i^{th} iteration, represented by m local centroids $f^i_{d,\text{LC}}$, are correlated with m global centroids $f^i_{d,\text{GC}}$ corresponding to the m clusters, which arise from each of the m ECG channels. Morphology and spectral content of cardiac signals vary gradually over time. Thus, in one approach, a new localized signal-dependent metric for the automatic quality assessment of the denoised ECG is obtained by assigning $f^i_{d,\text{GC}}$ to be the mean value of a finite set of prior local centroids for each channel. The mean square error (MSE) in an iteration is defined by the sum of the Euclidean distance between the centroids $f^i_{d,\text{GC}}$ and $f^i_{d,\text{LC}}$ for each of the m channels.

The threshold for the $\mathbf{K}(\mathbf{s})/\sigma^2_{\bar{\mathbf{Y}}}$ index (before the IC denoising block in Fig. 3) is gradually incremented in every iteration starting from its minimum value in the each frame. A greedy search algorithm thus identifies the correct value of a threshold, which achieves the minimum MSE (MMSE) solution. Thus, optimal denoising of the current frame is

Algorithm 1 Temporally-tuned Quality Assessment (TTQA)

Require: $N \geq 2f_s$; calibration centroid $f_{d,\text{CAL}} \neq 0$
Ensure: min $\|f_{d,\text{GC}} - f_{d,\text{LC}}\|^2$ {MMSE}
1: $\mathbf{s} \leftarrow \text{ICA}(\mathbf{x_n})$; $f_{d,\text{GC}} = f_{d,\text{CAL}}$; MMSE $= \infty$ {Initialize}
2: $\mathbf{L} := \text{SORT}(\mathbf{K}(\mathbf{s})/{\sigma_\mathbf{Y}}^2)$ {Sorted index list}
3: **for** $j = 1 :$ length$(\mathbf{L})$ **do**
4: $\quad\hat{\mathbf{A}}_\mathbf{d}^{-1} \leftarrow 0 \;\forall\; \mathbf{L} < \mathbf{L}(j)$ {Set null columns}
5: $\quad\mathbf{x}'_\mathbf{d} = \hat{\mathbf{A}}_\mathbf{d}^{-1}\mathbf{s}$ {Denoise}
6: $\quad f^i_{d,\text{LC}} \leftarrow \text{SFE}(\mathbf{x}'_\mathbf{d})$ {or MFE$(\mathbf{x}'_\mathbf{d})$}
7: $\quad\text{MSE} = \|f^i_{d,\text{GC}} - f^i_{d,\text{LC}}\|^2$
8: $\quad$**if** MSE $<$ MMSE **then**
9: $\quad\quad\mathbf{x_d} \leftarrow \mathbf{x}'_\mathbf{d}$; MMSE $\leftarrow$ MSE; $f^i_{d,\text{GC}} \leftarrow G\left(f^i_{d,\text{LC}}\right)$ {Update}
10: $\quad$**end if**
11: **end for**

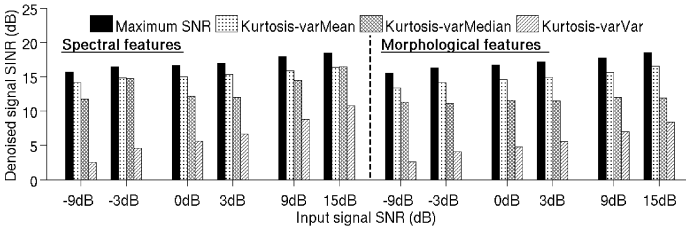

Fig. 4: A Kurtosis-VarMean based index is more robust than that based on Kurtosis-VarVar [8] and Kurtosis-VarMedian.

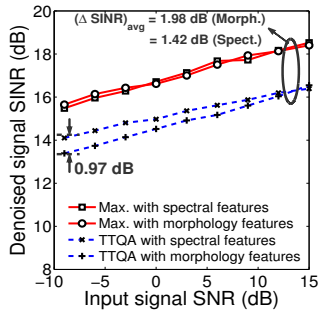

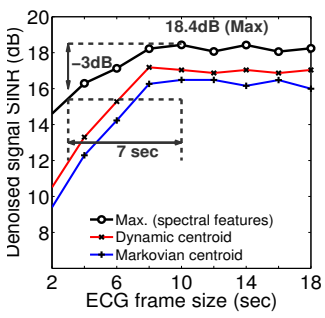

Fig. 5: TTQA-based denoising is robust with MFE and SFE.

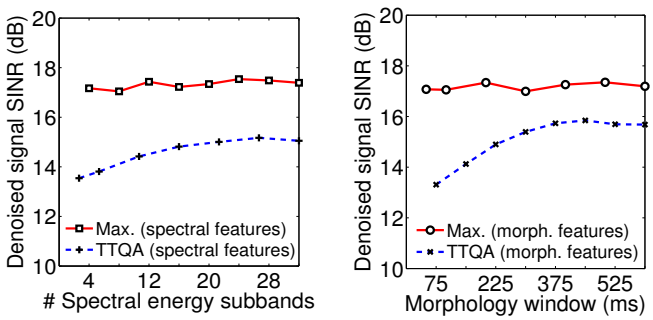

Fig. 6: Increased frame size, spectral or temporal resolution of feature extraction does not indefinitely improve denoising efficiency.

achieved by eliminating the set of ICs in the noise space while retaining useful components in the expected signal space.

A pseudo-code for the self-tracking TTQA algorithm is shown in Algorithm 1. After denoising a given frame, several approaches, based on a transformation G applied to $f^i_{d,\text{LC}}$, could be used to update $f^i_{d,\text{GC}}$. The trade-offs associated with three strategies are discussed in Sec. IV-A. During the initialization phase, a feature vector $f_{d,\text{CAL}}$, which is derived from a clean ECG signal forms a calibration seed for the global centroid.

IV. Experimental Results

The MIT-BIH noise stress test (NST) [14] database provides typical recordings of noise in ambulatory ECG. Calibrated amounts of noise from this database is added to 549 records of 1 kHz ECG from 249 patients in the PTB database. Fig. 4 shows the ability of TTQA in denoising ECG data thus obtained. It is observed that a $\mathbf{K(s)}/\sigma^2_{\mathbf{Y}}$-based index achieves an SINR close to that attainable by eliminating the ICs using a brute force search (denoted by Max. SNR). SINR in dB units is defined as $20.\log[\mathbf{P(x_e)}/\mathbf{P(x_d - x_e)}]$, where $\mathbf{P}(\cdot)$ represents the power of the signal, and $\mathbf{x_e}$ is the expected ECG signal, which is available as a baseline for validation from the PTB database (note that the expected signal is not accessible in a practical application). From the figure, it is also observed that the Kurtosis-VarMean based index is more robust than that based on Kurtosis-VarVar and Kurtosis-VarMedian.

Fig. 5 shows that the morphological and spectral features have a similar denoising performance. The denoising algorithm is almost insensitive to the input signal SNR since statistical independence exists even in the presence of large amplitudes of noise. For the evaluations in Figs. 4 and 5, a four second frame is used along with 5 leads (*viz. I*, *II*, *III*, *aVR*, and *aVL*) of ECG from the PTB database.

Variation of system parameters. Fig. 6 (at the left) shows a saturation in SINR gains with large frame sizes. Increased spectral resolution by the use of a larger number of energy bins does not show an improvement in the denoising efficiency (center in Fig. 6). A similar behavior of diminishing returns is observed with increased temporal resolution of the morphological features by the use of extra samples around the fiducial points for $f^i_{d,\text{LC}}$ (right of Fig. 6).

A. Denoising with a Dynamic Centroid.

After denoising a given frame, the global cluster centroids are updated based on a finite set of prior local centroids. In this section, we will explore the merits and demerits of the following three global centroid update functions G:

$$f^i_{d,\text{GC}} = G(f_{d,\text{LC}}) = \begin{cases} f^i_{d,\text{LC}}, & \text{if Markovian,} \\ f_{d,\text{CAL}}, & \text{if static,} \\ \left(\sum_{i=1}^{N} f^i_{d,\text{LC}}\right)/N & \text{if dynamic.} \end{cases} \quad (4)$$

The Markovian update process has a large error sensitivity since a sub-optimally denoised frame leads to a cascade of poorly denoised frames. In the static update function, a calibration frame ($f_{d,\text{CAL}}$ or initialization frame with no artifacts in the measured ECG) is used as a global template. Although this alleviates the problem of error-propagation, it does not accurately capture the evolving patient physiology. Thus, the optimal TTQA employs a dynamic update function where the global centroid is assigned to be the mean of the local centroid of a finite set of N prior frames.

The loci of the centroid functions are illustrated in Fig. 7 using a sample patient (patient #122) from the PTB database. Average results over the entire database, shown in Fig. 8, validate the superiority of the dynamic centroid. Further, dynamic update of $f^i_{d,\text{GC}}$ thus results in a smaller mean MMSE of 0.35 mV across 0.6 Million ECG frames of four seconds each. This corresponds to a 25.9% and 29.4% improvement

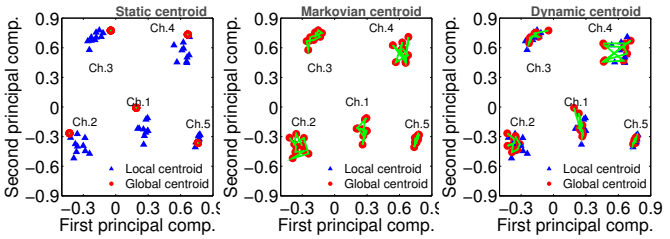

Fig. 7: Loci of the global centroids illustrate that a dynamic centroid accurately captures the evolving patient physiology.

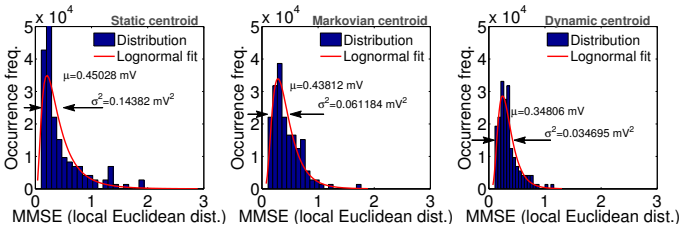

Fig. 8: A near-zero mean and variance of the MMSE in the PTB database shows the efficacy of a dynamic global centroid.

Table II: Arrhythmia classification [10] and beat detection [11] show stronger resilience to noise after TTQA.

Evaluation on AHA database							
SNR	**Q Se (%)**	**Q +P (%)**	**V Se (%)**	**V +P (%)**	**V FPR**	**# QRS**	**# VEB**
Baseline	**99.78**	**99.87**	**93.43**	**98.25**	**0.169**	**354324**	**32544**
TTQA	**99.78**	**99.87**	**93.43**	**98.51**	**0.150**	**354324**	**32620**
-9 dB	90.56	90.64	84.79	89.41	0.266	321561	29609
TTQA	99.69	99.78	93.34	98.42	0.160	353981	32597
-3 dB	92.02	92.08	86.17	90.84	0.234	326742	30082
TTQA	99.71	99.81	93.38	98.45	0.150	354018	32598
0 dB	93.29	93.35	87.35	92.09	0.216	331273	30496
TTQA	99.72	99.83	93.39	98.45	0.150	354109	32602
+3 dB	94.31	94.38	88.32	93.10	0.210	334905	30830
TTQA	99.72	99.82	93.39	98.45	0.150	354046	32600
+9 dB	99.65	99.73	93.32	98.18	0.174	353952	32581
TTQA	99.75	99.86	93.42	98.29	0.150	354289	32613

over the use of Markovian and static centroids, respectively. A smaller variance in the MMSE is also observed from Fig. 8.

V. Arrhythmia Classification and Beat Detection

In this section, we present a case study of arrhythmia classification, which demonstrates the ability of TTQA to preserve morphological information in the denoised ECG. The performance of a state-of-the-art, commercial arrhythmia detection software [15] using the AHA database [16] is shown in Table II. Results are presented according to the ANSI/AAMI EC57 specification standard [17]. Using the original AHA database, the sensitivity values for the classification of normal (Q Se) and ventricular ectopic beats (V Se) are 99.78 and 93.43%, respectively. The corresponding positive predictivity (+P) values are 99.87% and 98.5%, respectively. These results are shown in Table II along with the false positive rate (V FPR), the total number of ventricular ectopic (VEB), and normal (QRS) beats detected by the classification software. As a sanity check, TTQA did not degrade the classification performance. Notice a small increase in predictivity and decrease in the false positives for the abnormal (VEB) beats. This is shown in the second row of Table II.

In our evaluation experiments, it is observed that the performance of the classification algorithm suffers heavily with the direct use of noisy recordings obtained by the superposition of signals from the MIT-BIH NST and the AHA databases. Table II shows the degradations in the performance of the classifier for input signal SNR values of -9 dB, -3 dB, 0 dB, +3 dB, and +9 dB. The detection results after TTQA are also shown below the corresponding SNR values, respectively. It is observed from the table that the classification accuracy degrades with decreasing input signal SNR. Denoising the ECG data by TTQA prior to classification, however, improves the classifier accuracy significantly. A decrease of 2% in Se or +P from the baseline is considered clinically significant. This experiment shows that diagnostic-grade beat classification accuracy is maintained by TTQA even in the presence of severe motion artifacts.

VI. Instantaneous Heart Rate Estimation

In our experiments with the PTB and AHA databases in the previous section, synthetic noise was added to create the noisy ECG signals. In this section, we describe a second, more realistic case-study, which demonstrates accurate IHR estimation using TTQA-denoised ECG obtained directly from subjects performing a set of pre-defined activities in the lab.

A. Evaluation platform

In this section, we describe the closed-loop evaluation platform we built to demonstrate accurate ECG-based IHR estimation after denoising by TTQA. Fig. 9 shows the sub-systems used in the platform. There are five electrodes on the subject (*viz.* RA, RL, LA, LL, and V) with three streams [*viz.* $LA-RA$, $LL-RA$, and $V - 0.33 \times (LA + RA + LL)$] transmitted over a proprietary ultra-wide band (UWB) radio link. The medical sub-system comprises an analog front-end (AFE) and an ADC from Texas Instruments [18]. The data is sampled at 500 Hz with 16-bits of resolution. An on board Actel Igloo FPGA [19] enables MAC packetization and efficient encoding for secure communication. The table on the right in Fig. 9 shows the specifications of the evaluation platform. A receiver test board is connected to a PC, which performs TTQA-based denoising in MATLAB. Thus, the low-power platform enables a continuous monitoring of ambulatory subjects and results in clean recordings obtained after TTQA-based denoising.

For the IHR experiments, a pulse rate monitor device from Nonin [20] is used to measure the expected IHR of subjects performing routine activities using a parallel link over

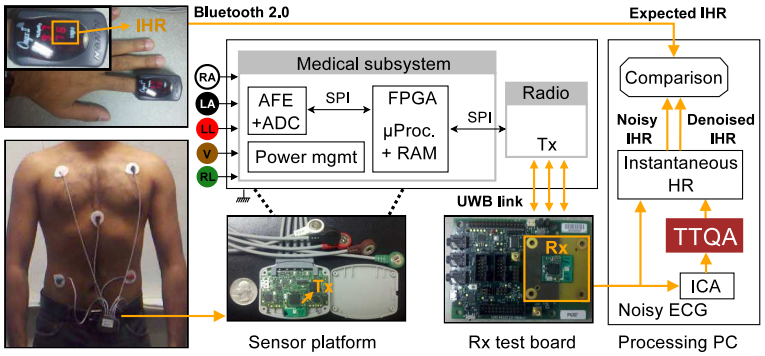

Specification		Comments
ECG config.	5-lead ECG (3 channels)	TI ADS-1194
Sampling rate	500 Hz, 16b/sample	Analog front-end + ADC
Sensor processing	Encoding, MAC packetization	Actel Igloo nano FPGA
Radio	Proprietary UWB ASIC	Pulse-position modulation
Data rate	8 × 132 Bytes per 256 ms = 33 kbps	Including application layer headers
Medical subsystem power	2.53 mW: 2.17 mW(FPGA core) 0.36 mW(I/O)	90% flash freeze on FPGA
Battery	387 mAHr (fast trickle charged)	2.5 days life (measured in lab) 24×7 continuous monitoring
Expected IHR (pulse monitor)	Range: 18-321 BPM Declared accuracy: ± 3%	Nonin OnyxII 9560 Bluetooth 2.0

Fig. 9: Table on the right shows specifications for the closed-loop IHR evaluation system. It comprises ECG acquisition by a low-power sensor platform followed by TTQA processing on a PC. ECG-based IHR is compared against expected measurements from Nonin Onyx II.

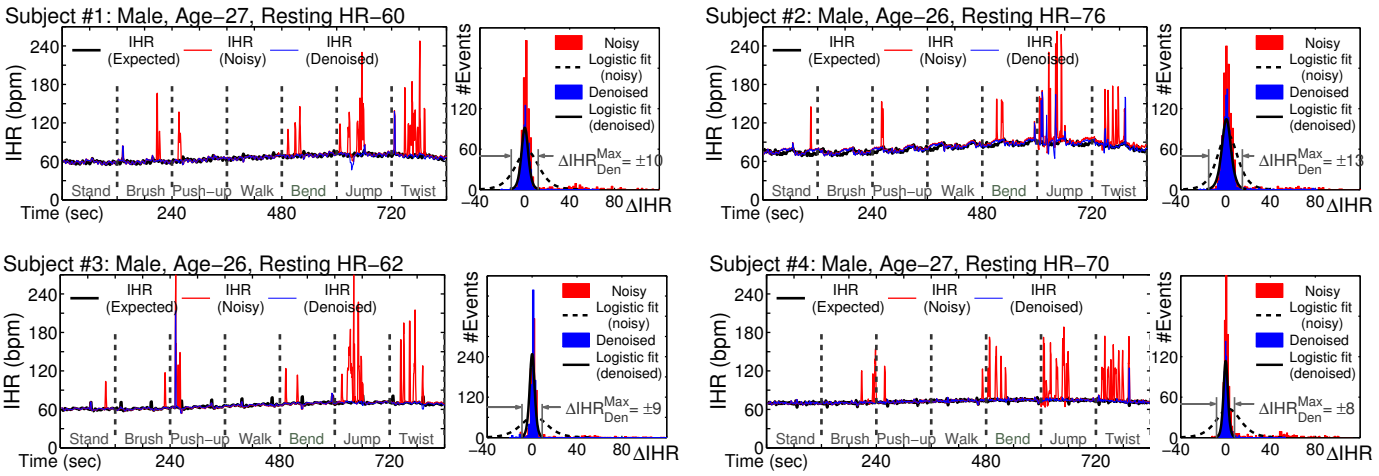

Fig. 10: Measures and estimates of IHR from four subjects performing routine activities show that TTQA-based denoising achieves accuracy within an average upper bound of ± 10 bpm while estimates with noisy recordings have an average upper bound of ±52 bpm.

Bluetooth 2.0. The expected IHR represents the ground truth, and is compared against the estimated IHR computed with the direct use of noisy ECG as well as that computed with the use of TTQA-denoised ECG. The IHR computation invokes a QRS detector based on a widely accepted algorithm [21]. Distance between the resulting fiducial points (RR-interval) is thus used to compute IHR according to the relationship, IHR = 60/(RR-interval in seconds).

Fig. 10 shows the expected IHR measurements and estimates derived from noisy ECG as well as those derived from TTQA-denoised ECG obtained from four subjects with no known prior pathological conditions. Each subject performed seven tasks for 60 seconds each preceeded by 60 seconds of inactivity. It is observed from the figure that TTQA-denoised ECG enables accurate IHR estimation with an average upper bound on the error being ±10 bpm (ΔIHR_{Den}^{Max}). The corresponding estimates with the direct use of noisy ECG results in an average error bound of ±52 bpm (ΔIHR_{Noi}^{Max}). The table below summarizes the observed reduction in the average RMS error from 47.7% to 7.0%.

	Subject #1	Subject #2	Subject #3	Subject #4
ΔIHR_{Noi}^{RMS}	31.3 bpm	30.9 bpm	31.4 bpm	33.1 bpm
ΔIHR_{Den}^{RMS}	5.0 bpm	6.4 bpm	3.6 bpm	3.9 bpm

VII. Conclusions

ICA-based mitigation of artifacts in current ECG monitoring systems is limited by (a) the inability to automatically identify independent components, which correspond to the sources of noise, and (b) the non-availability of a metric to assess the quality of the denoised ECG. We presented a technique to overcome the above limitations enabling a closed-loop validation of the denoised ECG using an algorithm based on temporal clustering. It was observed that the proposed TTQA algorithm retains fidelity in the ECG morphology corresponding to the evolving patient physiology. We presented a validation based on two case studies where we showed that ECG-denoising by TTQA prior to arrhythmia detection and instantaneous heart rate estimation improves the performance of state-of-the-art algorithms, even in the presence of severe motion artifacts.

References

[1] D Estrin *et al.*, "Connecting the physical world with pervasive networks," *IEEE Pervasive Computing*, pp. 59–69, Mar. 2002.

[2] N. V. Thakor and Y.-S. Zhu, "Applications of adaptive filtering to ECG analysis: Noise cancellation and arrhythmia detection," *IEEE Tran. Biomed. Engineering*, vol. 38, no. 8, pp. 785–794, Aug. 1991.

[3] G M. Friesen *et al.*, "A comparison of the noise sensitivity of nine QRS detection algorithms," *IEEE Trans. Biomed. Engineering*, vol. 37, no. 1, pp. 85–98, 1990.

[4] P. S. Hamilton, M. G. Curley, R. M. Aimi, and C. Sae-Hau, "Comparison of methods for adaptive removal of motion artifact," in *Comp. in Cardiology*. IEEE, 2000, pp. 383–386.

[5] C. J. James and C. W. Hesse, "Independent component analysis for biomedical signals," *Phys. Measurement*, vol. 26, pp. 15–39, 2005.

[6] M. Milanesi *et al.*, "Independent component analysis applied to the removal of motion artifacts from the electrocardiographic signals," *Med. and Bio. Engineering and Computing*, vol. 46, no. 3, pp. 251–261, 2008.

[7] R. Sameni, C. Jutten, and M. B. Shamsollahi, "What ICA provides for ECG processing: Application to noninvasive fetal ECG extraction," in *Proc. Symp. Signal Proc. and Info. Tech.*, Aug. 2006, pp. 656–661.

[8] T. He, G. Clifford, and L. Tarassenko, "Application of ICA in removing artifacts from the ECG," *J. Neural Computing Appl.*, vol. 15, no. 2, pp. 105–116, Apr. 2006.

[9] A Acharyya *et al.*, "Robust channel identification scheme: Solving permutation indeterminacy of ICA for artifacts romoval from ECG," in *Proc. Int. Conf. Engg. in Medicine and Bio.*, Aug. 2010, pp. 1142–1145.

[10] A. Hyvärinen and E. Oja, "Independent component analysis: Algorithms & appl." *J. Neural Networks*, vol. 13, no. 4-5, pp. 411–430, Jun. 2000.

[11] Physionet, "PTB diagnostic ECG database," http://www.physionet.org/physiobank/database.

[12] A. Hyvärinen and E. Oja, "A fast fixed-point algorithm for independent component analysis," *J. Neural Computation*, vol. 9, no. 7, pp. 1483–1492, Oct. 1997.

[13] J. Himberg, A. Hyvärinen, and F. Esposito, "Validating the independent components of neuroimaging time series via clustering and visualization," *J. Neuroimaging*, vol. 22, no. 3, pp. 1214–1222, Jul. 2004.

[14] Physionet, "MIT-BIH Noise Stress Test database," http://www.physionet.org/physiobank/database.

[15] Mortara, "VERITAS arrhythmia and ST segmentation analysis software," http://www.mortara.com/products/healthcare/veritas-algorithm.

[16] ECRI, "American heart association (AHA) ECG database," http://www.ecri.org/.

[17] ANSI/AAMI, "EC57: testing & reporting performance results of cardiac rhythm & ST-segment measurement algorithms," http://www. aami.org/.

[18] Texas Instruments Inc., Apr. 2011, "Low-power, 8-channel, 16-bit analog front-end for biopotential meas." http://www.ti.com/ product/ads1194.

[19] Actel Inc., Aug. 2010, "IGLOO nano low-power flash FPGA," http://www.actel.com/products/igloonano.

[20] Nonin Medical Inc., Jul. 2010, "Fingertip pulse oximeter," http://www.nonin.com/Onyx9560.

[21] J. Pan and W. J. Tompkins, "A real time QRS detection algorithm," *IEEE Trans. Biomedical Engineering*, vol. BME-32, no. 3, pp. 232–236, 1985.